PHYSICAL REVIEW APPLIED **18,** 034012 (2022)

Modulating Spin Polarization and Spin-Orbit Interaction by Submonolayer Engineering at $LaAlO_3/SrTiO_3$ Interfaces

Yan Hong,[1,*,‡] Marc-André Rose,[1] Zhaoting Zhang,[2] Ming Li,[3] Lisa Heymann,[1] Suqin He,[1] and
Felix Gunkel[1,†]

[1] *Peter Grünberg Institut 7 and JARA-FIT, Forschungszentrum Jülich, Jülich 52425, Germany*
[2] *Shaanxi Key Laboratory of Condensed Matter Structures and Properties and MOE Key Laboratory of Materials Physics and Chemistry under Extraordinary Conditions, School of Physical Science and Technology, Northwestern Polytechnical University, Xi'an 710072, China*
[3] *College of Chemistry and Chemical Engineering, Jishou University, Hunan 416000, China*

(Received 24 February 2022; revised 22 June 2022; accepted 28 July 2022; published 6 September 2022)

Recently, the $LaAlO_3/SrTiO_3$ (LAO/STO) interface has been highlighted as a major platform for spintronics, and its fundamental control of spin properties, therefore, becomes a key issue for application of this system. Here, we present a study showing the modulation of magnetic two-dimensional electron gases (2DEGs) with simultaneously enhanced spin-orbit interaction at the interface of LAO/STO by inserting $LaCoO_3$ submonolayers. At first, transport experiments provide evidence that Kondo behavior can be well controlled below about 13 K with the interlayer Co ions contributing as scattering centers. In addition, the systematic variation of the anomalous Hall effect obtained with increasing fraction of interfacial Co concentration below 10 K reveals that the spin polarization of 2DEGs is enhanced via submonolayer insertion. Simultaneously, we also observe an enlarged spin-orbit interaction at the buffered LAO/STO interface, resulting in a remarkably strong field-orientation-dependent magnetoresistance. Such tailored LAO/STO interfaces could potentially contribute to stronger spin-to-charge conversion responses and spin-torque measurements. Our observations indicate the subunit-cell insertion of functional layers to be a suitable route to tailor spin, orbital, and lattice interactions of the interfacial 2DEG, which makes the LAO/STO system an intriguing platform for spintronic applications.

DOI: 10.1103/PhysRevApplied.18.034012

I. INTRODUCTION

The two-dimensional electron gas (2DEG) at the interface of epitaxially grown $LaAlO_3$ (LAO) on TiO_2-terminated $SrTiO_3$ (STO) [1] has attracted much attention in recent years due to its extraordinary physical properties, such as spin-orbit coupling (SOC) [2,3], ferromagnetism [4–6], and superconductivity [7], which could pave the way for developing future electronic devices. Generally, the 2DEG at STO-based interfaces is confined in an asymmetric quantum well located on the STO side. The absence of spatial inversion symmetry at the heterointerfaces leads to strong Rashba SOC [8–10]. In recent years, 2DEGs at the interfaces between nonmagnetic oxides became appealing for the prospect of magnetic ordering because of their potential ability to support the emergence of quantum phases, promising the possibility to gain a spin-polarized 2DEG for spintronics [11]. In general, the anomalous Hall effect (AHE), as convincing evidence of ferromagnetic order in conducting materials, is observed only at very low temperatures [12,13]. Ben Shalom *et al.* detected the AHE at 20 mK at the LAO/STO interface [12]. Recently, the temperature for obtaining the AHE was improved to 30 K at a 1-nm $La_{7/8}Sr_{1/8}MnO_3$-buffered LAO/STO [14]. So far, to fabricate and improve ferromagnetic 2DEGs, various attempts, such as defect control [15,16], doping [17,18], and inserting ultrathin magnetic materials as a buffer layer, have been applied [14,19,20]. A hysteresis in the magnetoresistance and controllable SOC strength can be observed [4,18].

Here, based on the approach of interface engineering with buffer layers, we introduce a $LaCoO_3$ (LCO) layer between LAO and STO to achieve enhanced spin polarization of the 2DEG. LCO thin films under tensile strain typically provide a ferromagnetic state at around 85 K that is caused by the magnetic moment associated with the cobalt transition-metal centers [21,22]. Therefore, we attempt to enhance the 2DEG spin polarization and spin-orbit interaction (SOI) without reducing carrier mobility

---

[*] yanhphy@163.com
[†] f.gunkel@fz-juelich.de
[‡] Present address: Department of Physics, Faculty of Science, National University of Singapore, Singapore 117551, Singapore.

via the proximity effect of the Co^{3+} ions located right at the interface. Keeping the LCO interlayer at and below one unit cell allows the insertion of Co ions without impeding the electrostatic boundary condition at the interface, which is responsible for 2DEG formation. Our results are consistent with a recent study that mainly investigated the effect of a thicker LCO buffer layer, while no anomalous Hall resistance was observed in Ref. [23]. Based on this submonolayer-insertion method, the high mobility of the interface is conserved well, and we find that the AHE contribution can be systematically increased when approaching a full unit cell of LCO at the interface, accompanied by an enlarged spin-orbit interaction and a strong field-orientation-dependent magnetoresistance.

II. EXPERIMENT DETAILS

A series of LAO/LCO/STO heterostructures are fabricated by pulsed laser deposition. (001)-Oriented STO substrates are etched with a HF buffered solution to get TiO_2-terminated surfaces, which are then annealed afterwards at 950 °C for 2 h. The LCO and LAO thin films are deposited at 650 °C with a laser repetition rate of 1 Hz. The LCO thin films, from low coverages ($\delta = 0.25$ u.c.) up to saturation coverage ($\delta = 1$ u.c.), are deposited under 0.053-mbar oxygen pressure with a laser fluence of 2.0 J/cm^2. The coverages of the LCO thin films are controlled by the number of laser pulses used for deposition. Subsequently, LAO thin films are deposited using a laser fluence of 1.5 J/cm^2 under an oxygen pressure of 1×10^{-4} mbar. The target-substrate distance is fixed at 5.5 cm. The thickness of the LAO layer is kept at 10 u.c. All depositions are monitored by reflection high-energy electron diffraction (RHEED), indicating a layer-by-layer growth mode. The growth rate is about 51 and 50 pulses/u.c. for LCO and LAO, respectively. After deposition, the samples are cooled at a constant rate of 10 °C/min at the deposition pressure, to allow for a re-equilibration of the heterostructures after the growth process [24]. Atomic force microscopy shows that all films exhibit an atomically smooth surface morphology (see the Supplemental Material [25]). Temperature-dependent magnetization data of 30-u.c. LCO thin film obtained at the same growth condition indicates that it undergoes a magnetic transition at 53 K. The lower ferromagnetic ordering temperature as compared to LCO bulk in our LCO film can be understood in terms of LCO film thickness (see the Supplemental Material [25]).

A mimicked Hall bar geometry is adopted for electric measurements and ultrasonic Al-wire bonding is used to electrically connect the samples, as sketched in the inset of Fig. 1(a) [15]. The samples are cut into stripes with a size of 1×5 mm^2. To ensure homogeneous current density, contacts for current injection (I^+, I^-) are across the entire width of the sample to ensure a homogeneous current density. Contacts for $R_{xx}(V_1^+, V_1^-)$ and $R_{xy}(V_1^+, V_2^-)$

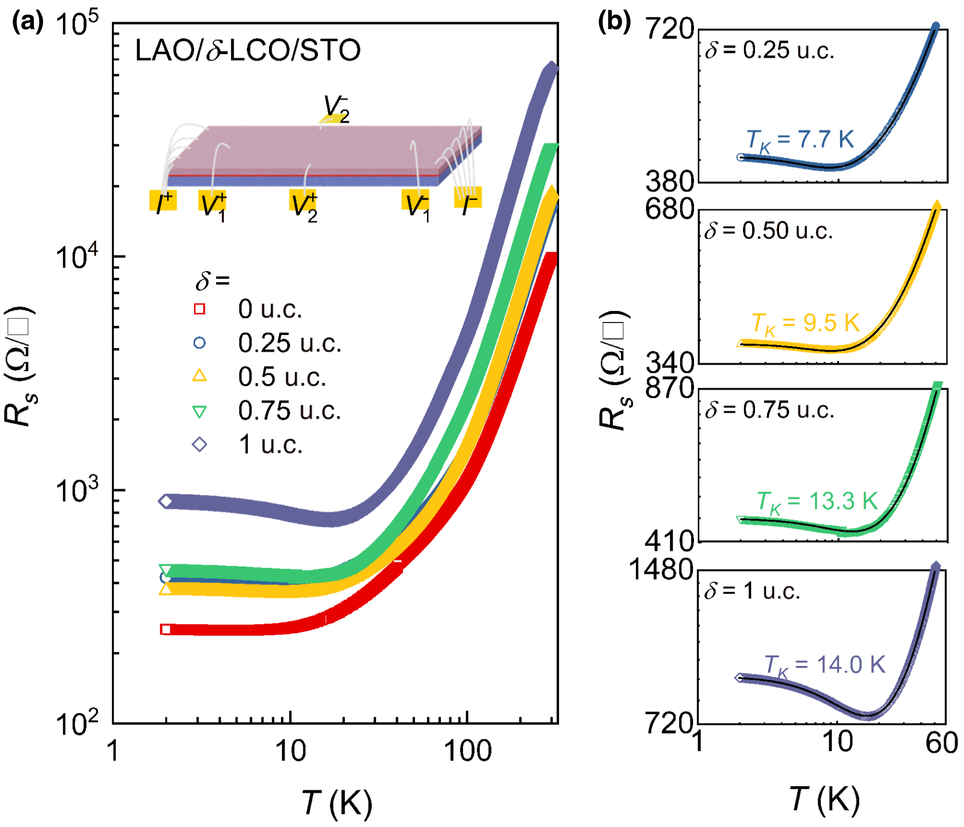

FIG. 1. (a) Temperature-dependent sheet resistance, R_s, of LAO/δ-LCO/STO heterostructures, where $\delta = 0$, 0.25, 0.5, 0.75, and 1 u.c. Inset, sketch of the measurement geometry. (b) Temperature-dependent R_s of inserted samples in the temperature range of 2–50 K is fitted by Kondo effect (solid lines).

measurements in four-point geometry are realized by single-wire bonds. Electric measurements are conducted in a Quantum Design physical property measurement system equipped with a 9-T superconducting magnet and a precision sample rotator. The system is able to apply temperatures in the range from 300 to 2 K.

III. RESULTS AND DISCUSSION

The electronic transport behavior at LAO/STO-based heterointerfaces is complex, with many potential and effective contributions to the overall transport. These typically require the combined analysis of different transport phenomena to capture the entirety of temperature-dependent resistance, Hall resistance (multiple carriers and AHE), and magnetotransport. It is often this multitude of phenomena that motivates the huge interest in complex oxide interfaces. First, we investigate the influence of the subinterlayer on the temperature dependence of the sheet resistance (R_s) of LAO/LCO/STO. Various LCO coverage layers, labeled as $\delta = 0$, 0.25, 0.5, 0.75, and 1 u.c., are prepared. Compared with the pristine sample ($\delta = 0$ u.c.), higher R_s is observed with higher LCO layer coverages, as depicted in Fig. 1(a). It can be seen from the R_s-T curves that the difference for partial coverages between $\delta = 0.25$- and 0.75-u.c. samples is not too large, indicating some sample-to-sample variations in R_s-T at intermediate coverages (see the Supplemental Material [25]). The $R_s(T)$ of the samples with $\delta = 0.25$, 0.5, 0.75, and 1 u.c. successively decreases when the temperature is lowered from 300 K to about 13 K, followed by an increase in resistance upon cooling below about 13 K. Finally, saturation is observed at the lowest temperatures. As shown by the solid lines in Fig. 1(b), the observed temperature dependence is consistent with a Kondo-type temperature dependence, as evident from a fit according to the standard formula [14,26,27]

$$R = R_0 + aT^b + R_K\left(\frac{1}{1+(2^{1/s}-1)(T/T_K)^2}\right)^s. \qquad (1)$$

Here, the parameters tabulated in Table I are adopted, where R_0 is the residual resistance, and the second term corresponds to the contribution from electron-electron and electron-phonon interactions. The last term in Eq. (1) corresponds to the Kondo contribution, where T_K is the Kondo temperature and R_K is the Kondo resistance at $T = 0$ K. It is important to note that slight sample-to-sample variations between similar samples would result in a slight variation of fitting parameters (see the Supplemental Material [25]). The determined T_K, however, is robust against these slight variations. The parameter s is close to 1.1, which is much larger than the usual value (0.225) obtained for Ti^{3+} ions [27]. This is consistent with the result of the manganite-buffered LAO/STO interface, where Mn ions are involved in the process of Kondo scattering [14]. In our work, obviously, Co ions contribute as scattering centers, considering their large magnetic moment. Over a temperature range of 2–50 K, T_K shifts toward a higher temperature with larger coverage, δ, from about 7.7 K for $\delta = 0.25$ u.c. to about 14.0 K for $\delta = 1$ u.c., while any Kondo upturn is absent in the pristine sample ($\delta = 0$ u.c.). The significantly lower T_K range, compared to the Curie temperature, indicates a much lower temperature range for the occurrence of magnetic polarization in the submonolayer buffer layers, which is consistent with the literature [14].

The enhanced Kondo-like behavior observed in the temperature dependence of the sheet resistance may indicate more pronounced magnetic scattering and potentially enhanced spin polarization of the 2DEGs with increasing LCO coverage. This effect, if it exists, should be reflected in the Hall resistance (R_{xy}). As an example, in Fig. 2(a), we show the magnetic field (B) dependence of R_{xy} of LAO/δ-LCO/STO ($\delta = 1$ u.c.), measured in the temperature range from 2 to 300 K. When the temperature is high (above 50 K), R_{xy} varies linearly with applied B, which is typical behavior for the normal Hall effect. When the sample is cooled to a low temperature below 50 K, the $R_{xy}(B)$ relationship becomes nonlinear. As reported previously, this behavior is attributed to a two-carrier contribution [28,29]. Based on this model, typically, the Hall coefficient, $R_H = R_{xy}/B$, obeys a Lorentzian-like shape with a single minimum at zero field. However, the R_H of our buffered samples below 10 K exhibits a clear upturn at low fields, rather than obeying a Lorentzian-like shape [plotted for comparison as orange lines in Fig. 2(b)], meaning that the two-band model alone cannot precisely describe our experimental Hall results [15,28,29]. Instead, experimental R_{xy} data are replicated exactly by summing two-carrier conduction, R_{xy}^{2e}, and AHE, R_{xy}^{AHE}, i.e., $R_{xy} = R_{xy}^{2e} + R_{xy}^{\mathrm{AHE}} = R_{xy}^{2e} + R_0^{\mathrm{AHE}}\tanh(B/B_c)$ [15]. Here, R_{xy}^{AHE} is expected to saturate at R_0^{AHE} when B is above a critical

TABLE I. Fitting parameters extracted from fitting R_s data of LAO/δ-LCO/STO ($\delta = 0$, 0.25, 0.5, 0.75, and 1 u.c.) heterointerfaces in Fig. 1(b) to Kondo model Eq. (1) in the temperature range of 2–50 K.

δ-LCO	R_0 ($\Omega/\square$)	a ($\Omega/\square\mathrm{K}^b$)	b	R_K ($\Omega/\square$)	s	T_K (K)
0	242.86	0.35	1.74	–	–	–
0.25	304.80	3.30	1.24	116.03	1.1 ± 0.01	7.7
0.5	277.14	1.41	1.45	94.09	1.1 ± 0.07	9.5
0.75	316.39	0.34	1.45	144.26	1.1 ± 0.01	13.3
1	443.88	0.46	1.96	457.45	1.1 ± 0.05	14.0

field (B_c). As we show in Fig. 2(c) (see the Supplemental Material [25]), experimental R_H data are well reproduced with the incorporation of an AHE component in the Hall coefficient (red lines), particularly the low-field upturn feature (see the Supplemental Material [25]). As illustrated in Fig. 2(d), the Hall resistance, R_{xy}, at 2 K is well separated into two parts: R_{xy}^{2e} (blue line) and R_{xy}^{AHE} (yellow line). In this case, R_{xy}^{2e} varies smoothly with B over the whole field range with a slight bending. Distinctively, R_{xy}^{AHE} is constant in the high-field range and undergoes a significant change as B approach low fields. By subtracting R_{xy}^{2e} from R_{xy}, we obtain the $R_{xy}^{\mathrm{AHE}} - B$ dependence as a function of temperature (see the Supplemental Material [25]). R_{xy}^{AHE} is positive when the magnetic field is positive and vice versa, which is consistent with the AHE observed in LAO/EuTiO$_3$/STO and NdGaO$_3$/STO [15,19].

Figures 2(e) and 2(f) show the temperature dependence of B_c and R_0^{AHE}, respectively, for different LCO interlayer coverages, δ. B_c is temperature independent in all samples and increases for higher buffer-layer coverages, δ, whereas R_0^{AHE} decreases with increasing temperature and vanishes above 8 K for $\delta = 0.25$ u.c. (above 10 K for $\delta > 0.25$ u.c.). By comparing AHE data of all samples, we find the largest value to be 55 Ω for the $\delta = 1$-u.c. sample and the smallest value to be 7.5 Ω for the $\delta = 0.25$-u.c. sample at 2 K. In contrast, only a very low AHE contribution is observed for the unbuffered LAO/STO ($\delta = 0$ u.c.) sample at 2–4 K (see the Supplemental Material [25]). As proven experimentally at complex oxide interfaces, more defects induced during growth can lead to a pronounced AHE [15]. This reveals that the unbuffered LAO/STO ($\delta = 0$ u.c.) sample represents a comparably low-defect concentration. The value is about 0.7 Ω at 2 K and takes up about 0.4% of the total R_{xy} at 9 T, which is far less than that of the $\delta = 1$-u.c. sample at 2 K (∼26.4%). Thus, the LCO buffer layer significantly enhances the AHE and increases the temperature for which the AHE occurs.

The carrier densities and mobilities as functions of temperature are extracted by using the two-band model (see the Supplemental Material [25]). In Figs. 3(a) and 3(b), we present the deduced carrier densities and mobilities for

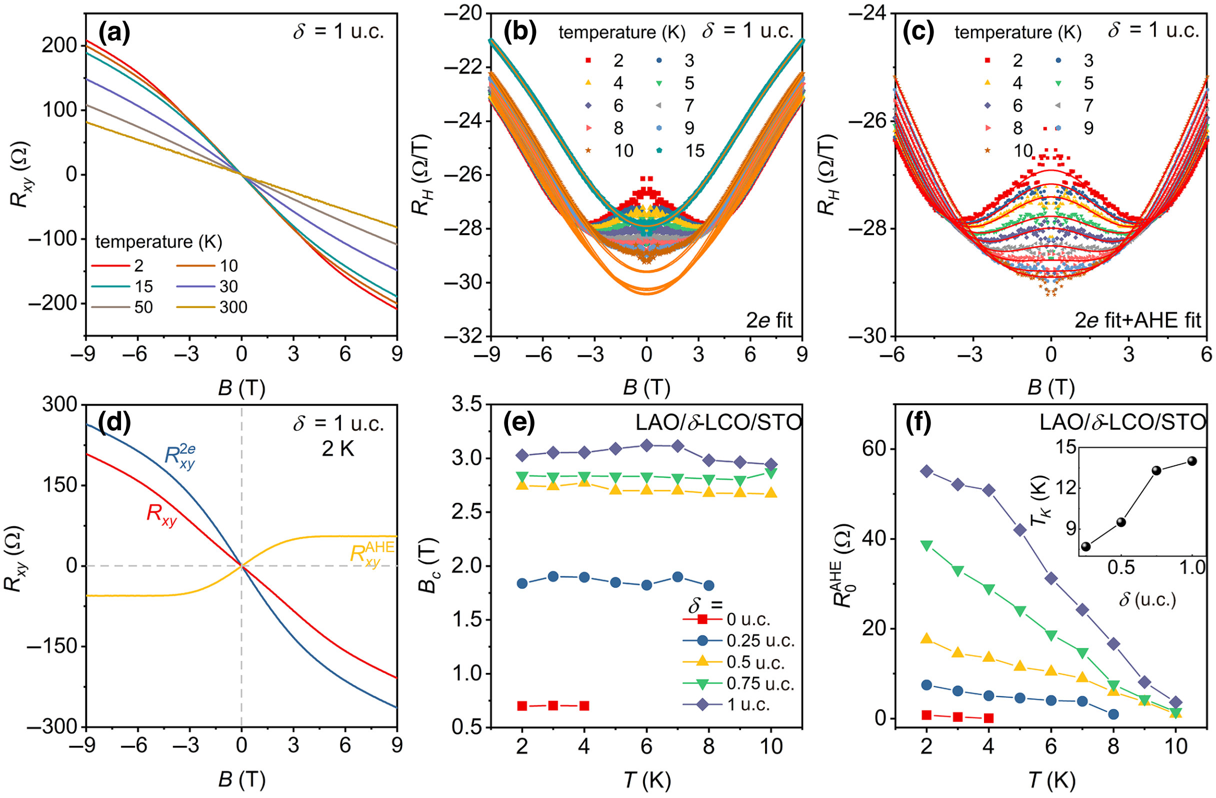

FIG. 2. (a) Magnetic field dependence of the Hall resistance (R_{xy}) for the LAO/δ-LCO/STO ($\delta = 1$ u.c.) interface measured in the temperature range from 2 to 300 K. (b) Hall coefficient, $R_H = R_{xy}/B$, obtained from data in (a) for $T = 2$ to 15 K. Fitting results according to the 2e model (orange solid lines) implies an obvious deviation from experimental data around low magnetic fields. (c) Fitting results of R_H around low fields in the same manner as displayed in (b) using the 2e model and an additional AHE contribution (red solid line). (d) Example for the determination of the 2e contribution (blue solid line) and AHE contribution (orange solid line) from the total Hall effect (red solid line) at 2 K for a LAO/δ-LCO/STO ($\delta = 1$ u.c.) sample. (e) Critical field, B_c, for the saturation of the AHE as a function of temperature. (f) Saturation resistance, R_0^{AHE}, as a function of temperature. Inset, δ dependence of the Kondo temperature (T_K).

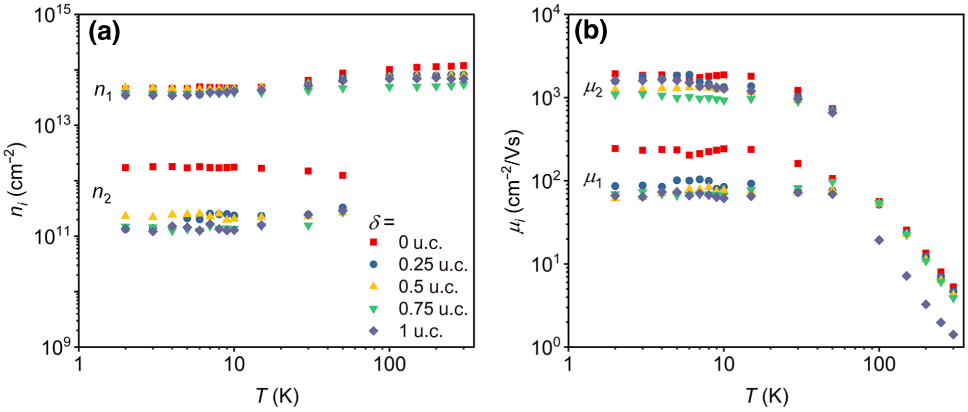

FIG. 3. (a),(b) Carrier density, n_i, and mobility, μ_i, of LAO/δ-LCO/STO, respectively, as a function of temperature, as determined by the two-band model with the AHE term based on the Hall effect. Two species of charge carrier coexist below 50 K.

LAO/δ-LCO/STO as a function of temperature. Only one kind of carrier is observed at high temperatures ($\gtrsim$100 K) with n around 3×10^{13} cm^{-2}. At low temperatures, there are two species of charge carriers in the 2DEG and, with the increasing temperature, the high-mobility carrier vanishes above 50 K. Notably, only the low carrier density (n_2) and low mobility (μ_1) of the two species of charge carriers show a slight decrease upon inserting the LCO buffer layer, from which we can speculate that we obtain an enhanced AHE without hampering the performance of the 2DEG.

We now turn to the influence of the buffer layer on longitudinal magnetotransport. Here, the magnetoresistance is defined as $\mathrm{MR} = (R_s(B) - R_s(0))/R_s(0) \times 100\%$. Figures 4(a)–4(c) demonstrates MR data for coverages $\delta = 0$, 0.5, and 1 u.c., respectively, with B applied perpendicular to both the sample plane and current direction. Data are labeled for the out-of-plane geometry as $\mathrm{MR}_\perp$.

A positive $\mathrm{MR}_\perp$ is observed at all temperatures for the $\delta = 0$-u.c. sample and increases during cooling to 2 K, where it is 40.3% at 9 T. This large $\mathrm{MR}_\perp$ is attributed to the enhanced transit path and scattering of electrons due to their cyclotron motion in the magnetic field. At low magnetic fields, $\mathrm{MR}_\perp$ is approximately parabolic with respect to B and follows the Kohler's rule ($\mathrm{MR}_\perp \propto aB^2$) [30,31], as shown in the inset of Fig. 4(a), which indicates the dominance of a classical orbital magnetoresistive effect induced by the Lorentz force. Disorder, in general, enhances the probability for electron-interference phenomena, such as weak (anti)localization, and therefore, might directly affect the observed transport behavior. Weak (anti)localization always occurs due to self-interference of electron wave functions, which can be best deduced from the field-dependent resistance changes and may also take place in parallel to Kondo-like changes in the scattering density. Note that the LAO/STO system, and particularly its magnetic structure, is shown to be laterally inhomogeneous [5] and electronic phase separation is observed [32], so different transport phenomena may occur even in parallel and add up to complex macroscopic transport behavior of the MR and its temperature behavior. Compared with the $\delta = 0$-u.c. sample, the $\mathrm{MR}_\perp$ of buffered samples is evidently lower under the same B. It is reduced to 20.0% and 15.0% at 2 K and 9 T for $\delta = 0.5$ and 1 u.c., respectively. Moreover, in the low-temperature range ($T \leq 5$ K), $\mathrm{MR}_\perp$ deviates from the quadratic field dependence observed at lower fields, as indicated by a cusp appearing near $B = 0$ T [Figs. 4(b) and 4(c)], which is a hint of the existence of weak antilocalization (WAL) [10,33,34]. The cusplike feature diminishes gradually with increasing temperature and vanishes above 5 K. The physical theory of the minimum in $\mathrm{MR}_\perp$ at $B = 0$ T is that a destructive interference effect of the coherently backscattered electrons effectively improves the conductivity of the 2DEG, which is suppressed by the applied out-of-plane B. Therefore, the resistance will increase sharply as the applied external B increases in the low-magnetic-field range [10]. We separate the contribution of classically positive MR by extrapolating the B^2 dependence seen at $B \geq 6$ T from the measured $R_{xx}(B)$. The resulting WAL contributions observed in MR are shown in Fig. S6 within the Supplemental Material [25]. A narrow minimum shows up, confirming that the SOC of the system is exceptionally strong [34]. In addition, the WAL component in the MR shows a smaller value at $B = 0$ with larger δ, reflecting a stronger SOC. This contribution can be expressed as [32,35,36]

$$\frac{\Delta R_{xx}(B)}{[R_{xx}(0)]^2} = -\frac{e^2}{2\pi^2\hbar}\left[\psi\left(\frac{1}{2} + \frac{B_\varphi}{B}\right) - \ln\frac{B_\varphi}{B}\right], \tag{2}$$

where $\Delta R_{xx}(B) = R_{xx}(B) - R_{xx}(0)$, $\psi(x)$ is the digamma function, R and $B_\varphi = \hbar/(4eL_\varphi^2)$. Our measured $\mathrm{MR}_\perp$ data of the inserted samples can be well described by the predictions of Eq. (2) as the solid lines shown as the inset in Figs. 4(b), 4(c), and Fig. S7 (see the Supplemental Material [25]) illustrate. The extracted $B_\varphi(T)$ and electron-dephasing length, $L_\varphi(T)$, are plotted in Figs. 4(d) and 4(e), respectively. The B_φ values increase as temperature increases and decrease with increasing LCO coverage. On the contrary, L_φ shows the opposite trend. It yields

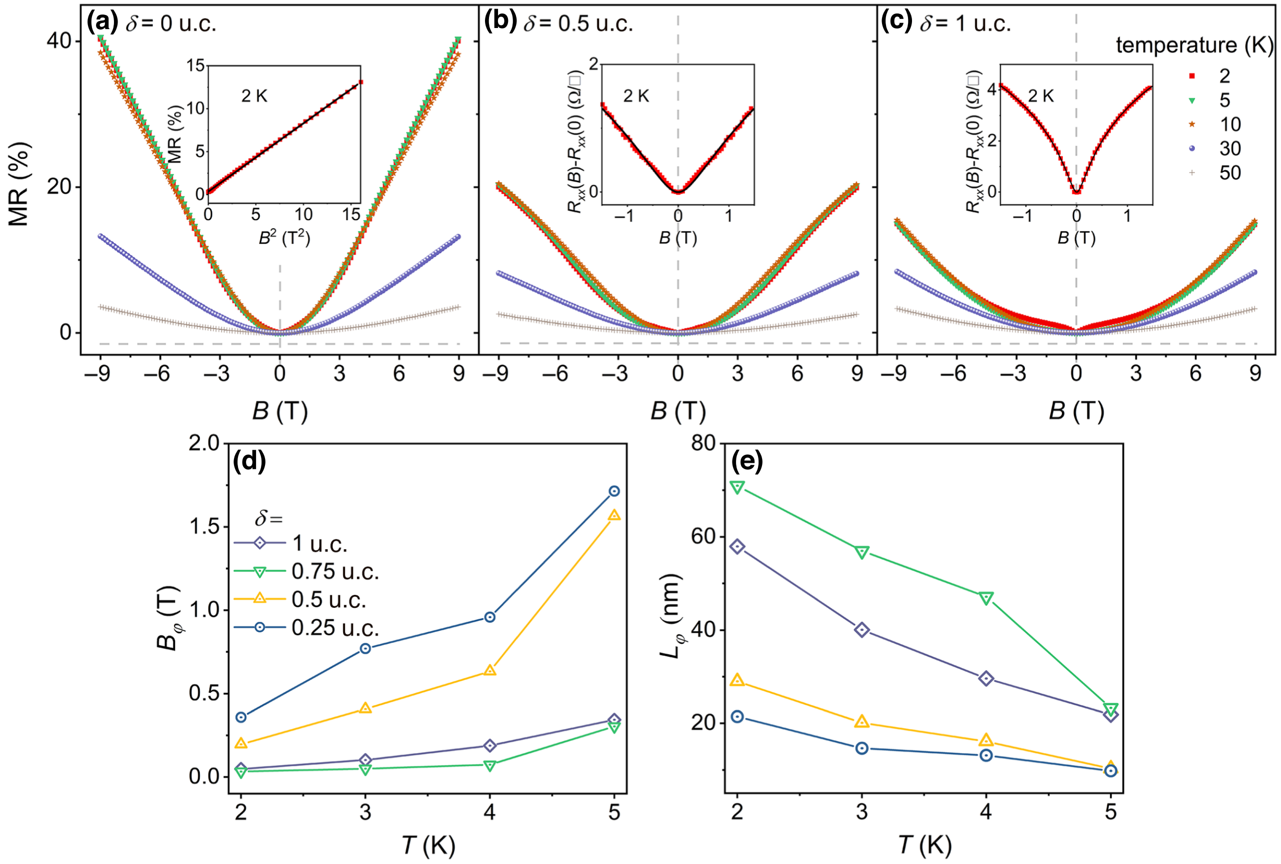

FIG. 4. (a)–(c) Out-of-plane magnetoresistance ($MR_\perp$) for coverages $\delta = 0$, 0.5, and 1 u.c., respectively. Inset in (a) shows a B^2 dependence of MR at 2 K for $\delta = 0$ u.c. Solid line represents the best linear fit of MR-B^2, indicating a dominating orbital effect. Insets in (b),(c) show low-field data at 2 K for $\delta = 0.5$ and 1 u.c. Solid curves are the theoretical predictions of Eq. (2). (d),(e) Variation of the extracted parameters B_φ and L_φ with temperature, respectively.

$L_\varphi \approx 29$ and 58 nm for $\delta = 0.5$ and 1 u.c., respectively, representing physically reasonable and cogent values, considering that the scattering is taking place in the plane with the film where L_φ has no dimensional constraints. Overall, these observed systematically changing parameters, i.e., T_K, WAL component, and characteristic field, demonstrate convincingly that disorder is gradually increased with larger δ.

In a parallel field, the orbital contribution to MR vanishes in 2D systems. However, the electrons can still interact with B via their spin. Thus, in a geometry where B is in plane of the 2DEG but aligned perpendicular to the direction of current, MR is labeled as $MR_{||}$. The $MR_{||}$ results for the $\delta = 0$-, 0.25-, 0.5-, 0.75-, and 1-u.c. samples are given in Figs. 5(a)–5(c) and S8 (see the Supplemental Material [25]), respectively. We see a striking difference in the field dependence of MR when the magnetic field is aligned parallel to the 2DEG plane. $MR_{||}$ is approximately zero at low fields and negative at high fields for the $\delta = 0$-u.c. sample (see the Supplemental Material [25]). As can be seen in Figs. 5(a)–5(c) for coverages of $\delta = 0.5$, 0.75, and 1 u.c., respectively, at low temperature, $MR_{||}$ consists of a positive slope at lower fields and a negative slope at higher fields for all samples, leading to a maximum value of $MR_{||}$, indicating a change from WAL to weak localization (WL) behavior. Similar behavior is observed for low-temperature transport results at LAO/STO interfaces, where charges in the ferromagnetic phase cause the in-plane resistance to drop at high magnetic fields [37,38].

In a WL-WAL system, an external magnetic field can break the time-reversal symmetry and reduce the interference of the time-reversal path, resulting in a dominant dynamic evolution of SOC and WL. With an increase of the magnetic field, SOC reduces the net interference contribution of forming the WAL to WL, which results in a sharply rising MR. Then, with a further increase of B, MR reaches its maximum value at the transition field (B_p), and the SOC no longer participates in quantum interference, indicating that B induces a WAL-WL transition. When B continues to increase, the MR decreases due to WL inhibition. The field and temperature dependence of $MR_{||}$ change significantly in buffered samples. The field value of the WAL-WL transition shifts to higher field with increasing coverage and decreasing

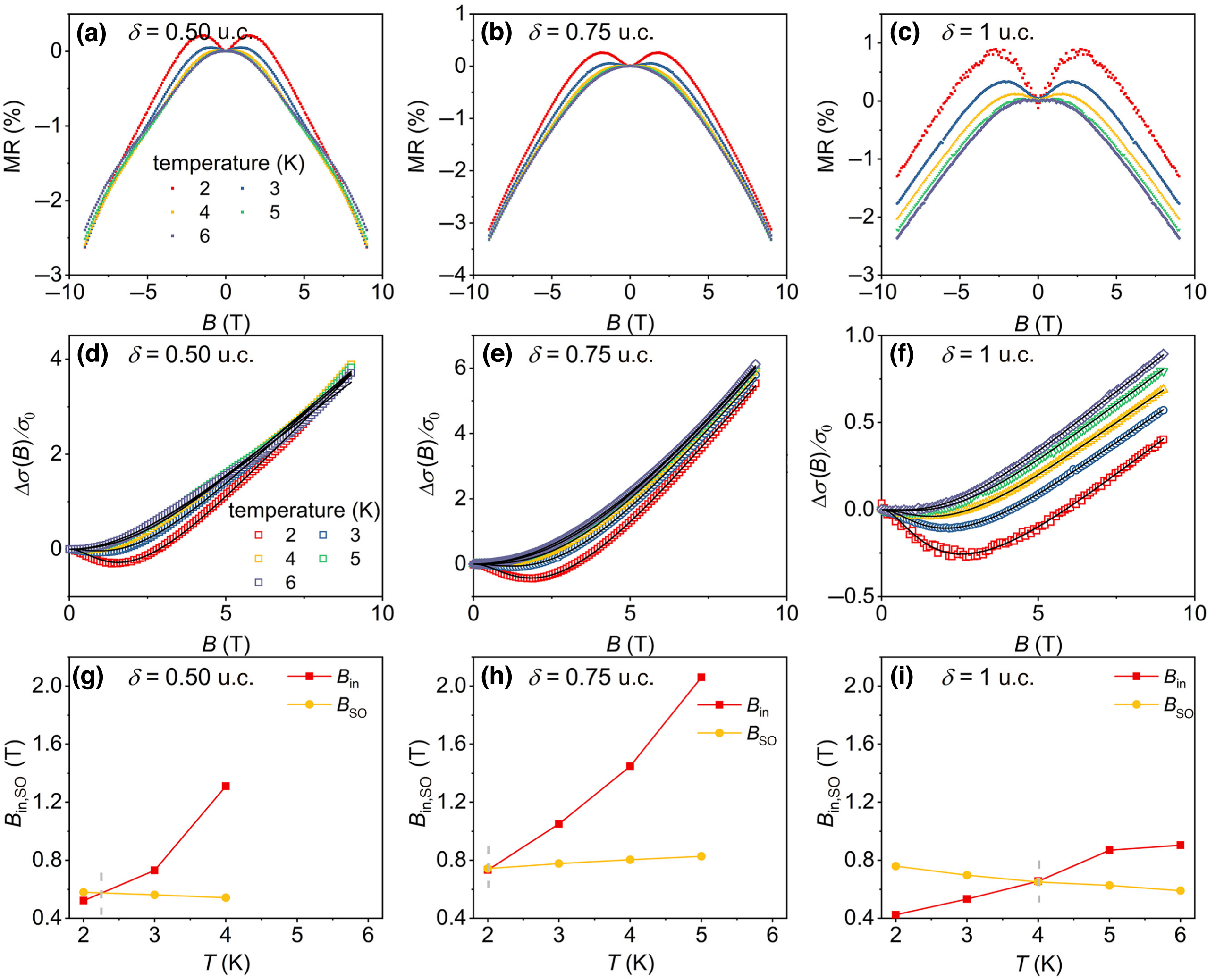

FIG. 5. (a)–(c) In-plane $\mathrm{MR}_{||}$ as a function of magnetic field in the low-temperature regime and sample coverages of $\delta = 0.5$, 0.75, and 1 u.c., respectively. (d)–(f) $\Delta\sigma/\sigma_0$ values as a function of magnetic field for coverages of $\delta = 0.5$, 0.75, and 1 u.c., respectively, shown as open symbols. Black solid lines are the fits obtained using Eq. (3). (g)–(i) Temperature dependence of characteristic magnetic fields (B_{in}, B_{SO}) for coverages of $\delta = 0.5$, 0.75, and 1 u.c., respectively.

temperature. The WAL-WL transition is derived from the quantum interference of coherent electron waves in the presence of spin relaxation (i.e., Rashba SOC), approximately reflecting the SOC strength [20]. When the temperature is increased to around 4, 5, and 6 K for coverages of $\delta = 0.5$, 0.75, and 1 u.c., respectively, the WAL effect becomes negligible, suggesting a much stronger Rashba SOC for higher buffered coverages. With a further increase of temperature, the SOC effect disappears completely, and the WL effect gradually weakens, showing a decreasing negative $\mathrm{MR}_{||}$. To understand the Rashba SOC effect more deeply and illustrate this behavior more quantitatively, the in-plane $\mathrm{MR}_{||}$ is normalized to the quantum conductance, as seen in Figs. 5(d)–5(f). Recent studies suggested that the WAL at the STO-based 2DEG system could be well described by two widely used theoretical models, Hikami-Larkin-Nagaoka and Iordanskii-Lyanda-Pikus [39,40]. Unfortunately, they are only valid for a perpendicular field and weak SOC. Hence, we apply the Maekawa-Fukuyama theory to analyze the WAL-WL, which can be expressed as [8,41]

$$\begin{aligned}\frac{\Delta\sigma(B)}{\sigma_0} &= \Psi\left(\frac{B}{B_{\mathrm{in}}+B_{\mathrm{SO}}}\right)\\ &\quad+\frac{1}{2\sqrt{1-\gamma^2}}\Psi\left(\frac{B}{B_{\mathrm{in}}+B_{\mathrm{SO}}\left(1+\sqrt{1-\gamma^2}\right)}\right)\\ &\quad-\frac{1}{2\sqrt{1-\gamma^2}}\Psi\left(\frac{B}{B_{\mathrm{in}}+B_{\mathrm{SO}}\left(1-\sqrt{1-\gamma^2}\right)}\right),\end{aligned} \tag{3}$$

where σ is the longitudinal conductance, obtained from the inversion of experimental resistance data; $\sigma_0(=e^2/\pi h)$ is the quantum of conductance and $\Delta\sigma(B) = \sigma(B) - \sigma(0)$. The function Ψ is defined as $\Psi(x) = \ln(x) + \psi((1/2) + (1/x))$, where $\psi(x)$ is the digamma function; B_{in} and B_{SO} are the characteristic magnetic fields related to inelastic scattering and spin-orbit scattering, respectively. The open symbols in Figs. 5(d)–5(f) are the conductance at various temperature for $\delta = 0.5$-, 0.75-, and 1-u.c. samples, respectively. The solid lines are the best-fit results using Eq. (3) with the known parameters (see the Supplemental Material [25]). We show only the curves for positive fields. The corresponding characteristic fields extracted from the best-fitting results are shown in Figs. 5(g)–5(i). The analysis reveals a nearly temperature-independent B_{SO} while B_{in} increases with increasing temperature. At low temperatures, we find that B_{SO} is larger than B_{in}, which indicates that WAL plays a dominant role at low temperatures. As the temperature increases, a crossover from $B_{\text{SO}} > B_{\text{in}}$ to $B_{\text{SO}} < B_{\text{in}}$ appears, indicating a transition from the dominant role being WAL to WL [42]. Remarkably, this crossover behavior does not appear in the R_s-T characteristics, which are dominated by the Kondo-like temperature dependence. We define the crossover temperature, T_{cross}, between WAL and WL as the temperature at which $B_{\text{in}} = B_{\text{SO}}$, signaling a change in the dominant scattering mechanism. T_{cross} shifts to higher temperatures with larger coverage. For $\delta = 0.5$- and 0.75-u.c. samples, the transition appears near 2 K. It increases to about 4 K for the $\delta = 1$-u.c. sample. The higher T_{cross} indicates a stronger Rashba SOC. The spin scattering (τ_{SO}) and the inelastic scattering (τ_{in}) times can be obtained by the relationships $B_{\text{in}} = \hbar/4eD\tau_{\text{in}}$ and $B_{\text{SO}} = \hbar/4eD\tau_{\text{SO}}$, respectively. For the $\delta = 0$-u.c. sample, the SOI is small, as indicated by the classical B^2 behavior of the MR. Therefore, τ_{in} and τ_{SO} can be considered nearly the same (around 1.0 ps, according to Ref. [32]). After inserting the δ layer, a much stronger effect of SOI is observed. The τ_{SO} drops around 2 orders of magnitude when $\delta = 1$ u.c. ($\tau_{\text{SO}} = 1.18 \times 10^{-2}$ ps) (see the Supplemental Material [25]). D is the diffusion coefficient. The spin-precession distance (L_{SO}) and the dephasing length (L_{in}) in the effective fields satisfy the condition $L_{\text{in,SO}} = \sqrt{\hbar/4eB_{\text{in,SO}}}$. This yields $L_{\text{in,SO}} \approx 19.7$ and 14.7 nm for the $\delta = 1$-u.c. sample at 2 K. This is smaller than the value of about 60 nm obtained on gated STO [43], reflecting a stronger SOC in LAO/δ-LCO/STO. In addition, the Rashba spin-splitting energy (Δ), which is around 5.5 meV (see the Supplemental Material [25]), shows an ignorable variation with increasingly buffered coverage.

The in-plane $\text{MR}_{||}$ for $\delta = 1$ u.c. in a geometry where the external field is parallel to the direction of current is labeled as $\text{MR}_{||||}$ and shows similar behavior to that of $\text{MR}_{||}$ (see the Supplemental Material [25]). The $B_{\text{in,SO}}$ is higher than that estimated from $\text{MR}_{||}$. In general, the MR behavior observed in buffered LAO/LCO/STO indicates the enlarged spin-orbit interaction and a remarkably strong field-orientation-dependent MR, as compared to the native LAO/STO heterointerface.

IV. CONCLUSION

We systematically investigate the LAO/STO interface by inserting a series of subunit-cell LCO buffer layers. The LCO submonolayer allows the insertion of Co ions right at the interface without hampering the interface's electrostatic boundary conditions. Therefore, its metallic properties are well preserved and the carrier concentrations and high mobilities of the 2DEG are not reduced but conserved well after inserting Co ions. At low temperatures, Kondo behavior, which is associated with Co ions, emerges and significantly increases with the increasing interfacial Co concentration. In addition, the spin polarization, reflected as an AHE contribution, is systematically enhanced with larger buffer-layer coverages. Both out-of-plane and in-plane MR data at low temperatures are analyzed in detail to extract the quantum contributions to electronic transport. The low-temperature MR suggests that the spin-orbit interaction of the system is exceptionally strong, which could support more efficient spin-to-charge conversion responses and spin-torque measurements [11]. Therefore, our study offers a perspective, i.e., inserting a subunit-cell magnetic layer, to tailor spin, orbital, and lattice interactions of the oxide 2DEG, making the high-performance spin-polarized LAO/STO system a promising platform for spintronic research and applications.

ACKNOWLEDGMENTS

H.Y. acknowledges support from the Sino-German (CSC-DAAD) Postdoc Scholarship Program, 2019 (Grant No. 201806290280). F.G. and M.R. acknowledge funding of Deutsche Forschungsgemeinschaft (DFG) through DFG GU/1604 (No. 315025796).

The authors declare no conflict of interest.

[1] A. Ohtomo and H. Y. Hwang, A high-mobility electron gas at the $LaAlO_3/SrTiO_3$ heterointerface, Nature **427**, 423 (2004).

[2] D. A. Dikin, M. Mehta, C. W. Bark, C. M. Folkman, C. B. Eom, and V. Chandrasekhar, Coexistence of Superconductivity and Ferromagnetism in Two Dimensions, Phys. Rev. Lett. **107**, 056802 (2011).

[3] H. Liang, L. Cheng, L. Wei, Z. Luo, G. Yu, C. Zeng, and Z. Zhang, Nonmonotonically tunable Rashba spin-orbit coupling by multiple-band filling control in $SrTiO_3$-based interfacial *d*-electron gases, Phys. Rev. B **92**, 075309 (2015).

[4] A. Brinkman, M. Huijben, M. van Zalk, J. Huijben, U. Zeitler, J. C. Maan, W. G. van der Wiel, G. Rijnders, D. H.

Blank, and H. Hilgenkamp, Magnetic effects at the interface between non-magnetic oxides, Nat. Mater. **6**, 493 (2007).

[5] B. Kalisky, J. A. Bert, B. B. Klopfer, C. Bell, H. K. Sato, M. Hosoda, Y. Hikita, H. Y. Hwang, and K. A. Moler, Critical thickness for ferromagnetism in $LaAlO_3/SrTiO_3$ heterostructures, Nat. Commun. **3**, 922 (2012).

[6] D. V. Christensen, Y. Frenkel, Y. Z. Chen, Y. W. Xie, Z. Y. Chen, Y. Hikita, A. Smith, L. Klein, H. Y. Hwang, N. Pryds, and B. Kalisky, Strain-tunable magnetism at oxide domain walls, Nat. Phys. **15**, 269 (2019).

[7] N. Reyren, S. Thiel, A. D. Caviglia, L. F. Kourkoutis, G. Hammerl, C. Richter, C. W. Schneider, T. Kopp, A. S. Ruetschi, D. Jaccard, *et al.*, Superconducting interfaces between insulating oxides, Science **317**, 1196 (2007).

[8] A. D. Caviglia, M. Gabay, S. Gariglio, N. Reyren, C. Cancellieri, and J. M. Triscone, Tunable Rashba spin-orbit interaction at oxide interfaces, Phys. Rev. Lett. **104**, 126803 (2010).

[9] Y. A. Bychkov and E. I. Rashba, Properties of a 2D electron gas with lifted spectral degeneracy, J. Exp. Theor. Phys. Lett. **39**, 78 (1984).

[10] A. Manchon, H. C. Koo, J. Nitta, S. M. Frolov, and R. A. Duine, New perspectives for Rashba spin-orbit coupling, Nat. Mater. **14**, 871 (2015).

[11] F. Trier, P. Noël, J. V. Kim, J. P. Attané, L. Vila, and M. Bibes, Oxide spin-orbitronics: Spin-charge interconversion and topological spin textures, Nat. Rev. Mater. **7**, 25 (2022).

[12] M. Ben Shalom, M. Sachs, D. Rakhmilevitch, A. Palevski, and Y. Dagan, Tuning Spin-Orbit Coupling and Superconductivity at the $SrTiO_3/LaAlO_3$ Interface: A Magnetotransport Study, Phys. Rev. Lett. **104**, 126802 (2010).

[13] A. Joshua, S. Pecker, J. Ruhman, E. Altman, and S. Ilani, A universal critical density underlying the physics of electrons at the $LaAlO_3/SrTiO_3$ interface, Nat. Commun. **3**, 1129 (2012).

[14] H. R. Zhang, Y. Zhang, H. Zhang, J. Zhang, X. Shen, X. X. Guan, Y. Z. Chen, R. C. Yu, N. Pryds, Y. S. Chen, *et al.*, Magnetic two-dimensional electron gas at the manganite-buffered $LaAlO_3/SrTiO_3$ interface, Phys. Rev. B **96**, 195167 (2017).

[15] F. Gunkel, C. Bell, H. Inoue, B. Kim, A. G. Swartz, T. A. Merz, Y. Hikita, S. Harashima, H. K. Sato, M. Minohara, *et al.*, Defect Control of Conventional and Anomalous Electron Transport at Complex Oxide Interfaces, Phys. Rev. X **6**, 031035 (2016).

[16] M. A. Rose, B. Smid, M. Vorokhta, I. Slipukhina, M. Andra, H. Bluhm, T. Duchon, M. Lezaic, S. A. Chambers, R. Dittmann, *et al.*, Identifying ionic and electronic charge transfer at oxide heterointerfaces, Adv. Mater. **33**, 2004132 (2021).

[17] P. Moetakef, J. R. Williams, D. G. Ouellette, A. P. Kajdos, D. Goldhaber-Gordon, S. J. Allen, and S. Stemmer, Carrier-Controlled Ferromagnetism in $SrTiO_3$, Phys. Rev. X **2**, 021014 (2012).

[18] P. Kumar, A. Dogra, P. P. Bhadauria, A. Gupta, K. K. Maurya, and R. C. Budhani, Enhanced spin-orbit coupling and charge carrier density suppression in $LaAl_{1-x}Cr_xO_3/SrTiO_3$ hetero-interfaces, J. Phys.: Condens. Matter **27**, 125007 (2015).

[19] D. Stornaiuolo, C. Cantoni, G. M. De Luca, R. Di Capua, E. Di Gennaro, G. Ghiringhelli, B. Jouault, D. Marre, D. Massarotti, F. Miletto Granozio, *et al.*, Tunable spin polarization and superconductivity in engineered oxide interfaces, Nat. Mater. **15**, 278 (2016).

[20] Y. Gan, Y. Zhang, D. V. Christensen, N. Pryds, and Y. Chen, Gate-tunable Rashba spin-orbit coupling and spin polarization at diluted oxide interfaces, Phys. Rev. B **100**, 125134 (2019).

[21] L. Qiao, J. H. Jang, D. J. Singh, Z. Gai, H. Xiao, A. Mehta, R. K. Vasudevan, A. Tselev, Z. Feng, H. Zhou, *et al.*, Dimensionality controlled octahedral symmetry-mismatch and functionalities in epitaxial $LaCoO_3/SrTiO_3$ heterostructures, Nano Lett. **15**, 4677 (2015).

[22] J. W. Freeland, J. X. Ma, and J. Shi, Ferromagnetic spin-correlations in strained $LaCoO_3$ thin films, Appl. Phys. Lett. **93**, 212501 (2008).

[23] R. S. Yang, H. Yin, M. Li, S. H. Wang, and K. X. Jin, Manipulating spin-orbit coupling at oxide interfaces by lanthanum cobaltate, ACS Appl. Electron. Mater. **4**, 1117 (2022).

[24] M. Lee, J. R. Williams, S. Zhang, C. D. Frisbie, and D. Goldhaber-Gordon, Electrolyte Gate-Controlled Kondo Effect in $SrTiO_3$, Phys. Rev. Lett. **107**, 256601 (2011).

[25] See the Supplemental Material at http://link.aps.org/supplemental/10.1103/PhysRevApplied.18.034012 for additional details of sample-surface morphology; Hall coefficient, R_H, obtained experimentally and corresponding theoretical predictions for all buffered samples; magnetic field dependence of deduced AHE contribution at different temperatures for $\delta = 1$ u.c.; temperature dependence of carrier density and mobility of LAO/δ-LCO/STO; the contribution of WAL to out-of-plane magnetoresistance at 2 K as a function of δ; out-of-plane magnetoresistance for all buffered samples; and in-plane magnetoresistance for $\delta = 0$ and 0.25 u.c.

[26] W. N. Lin, J.-F. Ding, S.-X. Wu, Y. F. Li, J. Lourembam, S. Shannigrahi, S. J. Wang, and T. Wu, Electrostatic modulation of $LaAlO_3/SrTiO_3$ interface transport in an electric double-layer transistor, Adv. Mater. Interfaces **1**, 1300001 (2014).

[27] J. S. Kim, S. S. A. Seo, M. F. Chisholm, R. K. Kremer, H. U. Habermeier, B. Keimer, and H. N. Lee, Nonlinear Hall effect and multichannel conduction in $LaTiO_3/SrTiO_3$ superlattices, Phys. Rev. B **82**, 201407 (2010).

[28] V. K. Guduru, A. McCollam, A. Jost, S. Wenderich, H. Hilgenkamp, J. C. Maan, A. Brinkman, and U. Zeitler, Thermally excited multiband conduction in $LaAlO_3/SrTiO_3$ heterostructures exhibiting magnetic scattering, Phys. Rev. B **88**, 241301 (2013).

[29] J. H. Ngai, Y. Segal, D. Su, Y. Zhu, F. J. Walker, S. Ismail-Beigi, K. Le Hur, and C. H. Ahn, Electric field tuned crossover from classical to weakly localized quantum transport in electron doped $SrTiO_3$, Phys. Rev. B **81**, 241307 (2010).

[30] J. Ding, J. Cheng, F. Dogan, Y. Li, W. Lin, Y. Yao, A. Manchon, K. Yang, and T. Wu, Two-dimensional electron gas at the spinel/perovskite interface: Suppression of polar catastrophe by an ultrathin layer of interfacial defects, ACS Appl. Mater. Interfaces **12**, 42982 (2020).

[31] M. Liu, Y. Hong, H. Xue, J. Meng, W. Jiang, Z. Zhang, J. Ling, R. Dou, C. Xiong, L. He, and J. Nie, Enhancement of Rashba spin-orbit coupling by electron confinement at the $LaAlO_3/SrTiO_3$ interface, J. Phys.: Condens. Matter **32**, 235003 (2020).

[32] Ariando, X. Wang, G. Baskaran, Z. Q. Liu, J. Huijben, J. B. Yi, A. Annadi, A. R. Barman, A. Rusydi, S. Dhar, *et al.*, Electronic phase separation at the $LaAlO_3/SrTiO_3$ interface, Nat. Commun. **2**, 188 (2011).

[33] S. Das, Z. Hossain, and R. C. Budhani, Signature of enhanced spin-orbit interaction in the magnetoresistance of $LaTiO_3/SrTiO_3$ interfaces on δ doping, Phys. Rev. B **94**, 115165 (2016).

[34] B. Grbić, R. Leturcq, T. Ihn, K. Ensslin, D. Reuter, and A. D. Wieck, Strong spin-orbit interactions and weak antilocalization in carbon-doped p-type $GaAs/Al_xGa_{1-x}As$ heterostructures, Phys. Rev. B **77**, 125312 (2008).

[35] S. Das, A. Rastogi, L. Wu, J. C. Zheng, Z. Hossain, Y. Zhu, and R. C. Budhani, Kondo scattering in δ-doped $LaTiO_3/SrTiO_3$ interfaces: Renormalization by spin-orbit interactions, Phys. Rev. B **90**, 081107 (2014).

[36] S. P. Chiu and J. J. Lin, Weak antilocalization in topological insulator Bi_2Te_3 microflakes, Phys. Rev. B **87**, 035122 (2013).

[37] H. Xue, C. Li, Y. Hong, X. Wang, Y. Li, K. Liu, W. Jiang, M. Liu, L. He, R. Dou, *et al.*, Temperature dependence of the conductive layer thickness at the $LaAlO_3/SrTiO_3$ heterointerface, Phys. Rev. B **96**, 235310 (2017).

[38] S. Hikami, A. I. Larkin, and Y. Nagaoka, Spin-orbit interaction and magnetoresistance in the two dimensional random system, Prog. Theor. Phys. **63**, 707 (1980).

[39] S. V. Iordanskii, Y. B. Lyanda-Geller, and G. E. Pikus, Weak localization in quantum wells with spin-orbit interaction, Sov. J. Exp. Theor. Phys. Lett. **60**, 206 (1994).

[40] S. Maekawa and H. Fukuyama, Magnetoresistance in two-dimensional disordered systems: Effects of Zeeman splitting and spin-orbit scattering, J. Phys. Soc. Jpn. **50**, 2516 (1981).

[41] H. Zhang, H. Zhang, X. Yan, X. Zhang, Q. Zhang, J. Zhang, F. Han, L. Gu, B. Liu, Y. Chen, *et al.*, Highly mobile two-dimensional electron gases with a strong gating effect at the amorphous $LaAlO_3/KTaO_3$ Interface, ACS Appl. Mater. Interfaces **9**, 36456 (2017).

[42] H. Nakamura, T. Koga, and T. Kimura, Experimental Evidence of Cubic Rashba Effect in an Inversion-Symmetric Oxide, Phys. Rev. Lett. **108**, 206601 (2012).

[43] C. C. Xu, H. C. Du, A. J. H. van der Torren, J. Aarts, C. L. Jia, and R. Dittmann, Formation mechanism of Ruddlesden-Popper-type antiphase boundaries during the kinetically limited growth of Sr rich $SrTiO_3$ thin films, Sci. Rep. **6**, 38296 (2016).